

Effect of Cavities on the Optical Properties of Bullet Rosettes: Implications for Active and Passive Remote Sensing of Ice Cloud Properties

PING YANG,* ZHIBO ZHANG,* GEORGE W. KATTAWAR,⁺ STEPHEN G. WARREN,[#] BRYAN A. BAUM,[@]
HUNG-LUNG HUANG,[@] YONG X. HU,[&] DAVID WINKER,[&] AND JEAN IAQUINTA**

**Department of Atmospheric Sciences, Texas A&M University, College Station, Texas*

+*Department of Physics, Texas A&M University, College Station, Texas*

#*Department of Atmospheric Sciences, University of Washington, Seattle, Washington*

@*Space Science and Engineering Center, University of Wisconsin—Madison, Madison, Wisconsin*
&*NASA Langley Research Center, Hampton, Virginia*

***Transport Research Laboratory, Wokingham, Berkshire, United Kingdom*

(Manuscript received 22 October 2007, in final form 31 January 2008)

ABSTRACT

Bullet rosette particles are common in ice clouds, and the bullets may often be hollow. Here the single-scattering properties of randomly oriented hollow bullet rosette ice particles are investigated. A bullet, which is an individual branch of a rosette, is defined as a hexagonal column attached to a hexagonal pyramidal tip. For this study, a hollow structure is included at the end of the columnar part of each bullet branch and the shape of the hollow structure is defined as a hexagonal pyramid. A hollow bullet rosette may have between 2 and 12 branches. An improved geometric optics method is used to solve for the scattering of light in the particle. The primary optical effect of incorporating a hollow end in each of the bullets is to decrease the magnitude of backscattering. In terms of the angular distribution of scattered energy, the hollow bullets increase the scattering phase function values within the forward scattering angle region from 1° to 20° but decrease the phase function values at side- and backscattering angles of 60° – 180° . As a result, the presence of hollow bullets tends to increase the asymmetry factor. In addition to the scattering phase function, the other elements of the phase matrix are also discussed. The backscattering depolarization ratios for hollow and solid bullet rosettes are found to be very different. This may have an implication for active remote sensing of ice clouds, such as from polarimetric lidar measurements. In a comparison of solid and hollow bullet rosettes, the effect of the differences on the retrieval of both the ice cloud effective particle size and optical thickness is also discussed. It is found that the presence of hollow bullet rosettes acts to decrease the inferred effective particle size and to increase the optical thickness in comparison with the use of solid bullet rosettes.

1. Introduction

In the past three decades, great strides have been made in the simulation of the single-scattering properties (i.e., the scattering phase matrix, extinction cross section, and single-scattering albedo) of nonspherical ice particles within ice clouds [see review by Yang and Liou (2006)]. The motivation for studying ice clouds is

their importance for understanding the earth's hydrological cycle. Additionally, ice clouds have a significant impact on the radiation budget in the earth-atmosphere system, and hence on climate (Liou 1986; Stephens et al. 1990; Lynch et al. 2002, and references cited therein). At present, the representation of these clouds in climate models is still quite crude in comparison with the case of water clouds that are assumed to consist of spherical liquid water droplets. Significant differences are found when simulations of ice clouds by climate models are compared to satellite observations (Zhang et al. 2005). To improve the parameterization of the bulk radiative properties of ice clouds, which is a

Corresponding author address: Dr. Ping Yang, Department of Atmospheric Sciences, Texas A&M University, TAMU 3150, College Station, TX 77843-3150.
E-mail: pyang@ariel.met.tamu.edu

necessary component of the radiative transfer schemes used in climate models, it is important to learn more about the optical properties of highly complex, nonspherical ice particles. The optical properties are determined fundamentally by the ice habits, particle size distributions, and refractive indices. Furthermore, modeling the optical properties of complex ice particles is also an interesting but challenging research topic in the discipline of electromagnetic scattering and computational physics.

In synoptic cirrus, ice particles tend to range from tens to hundreds of microns in size. In regions of intense convection, however, ice particles can become much larger. Thus, the principles of geometric optics, particularly the ray-tracing technique based on Snell's law, the Fresnel formulas, and the Fraunhofer diffraction approximation, can be used to derive the scattering properties of these particles at visible and near-infrared wavelengths because of the ensuing large size parameters. At infrared wavelengths, the strong absorption of ice complicates the implementation of the ray-tracing technique because of the inhomogeneous properties of the localized waves within the scattering particles (Yang et al. 2001; Chang et al. 2005), although this effect is usually neglected in many studies reported in the literature. After the pioneering studies of Jacobowitz (1971), Wendling et al. (1979), and Cai and Liou (1982), the ray-tracing technique has been employed extensively to investigate the interaction between electromagnetic radiation and nonspherical ice particles with size parameters in the geometric optics regime. However, the scattering of light by nonspherical ice particles has also been investigated with other approaches (Mishchenko and Sassen 1998; Yang and Liou 1996a; Sun et al. 1999; Baran et al. 2001; Mitchell et al. 2006). The early ray-tracing studies focused on the case of pristine hexagonal ice plates and columns that were solid ice particles with smooth faces (e.g., Takano and Jayaweera 1985; Takano and Liou 1989; Rockwitz 1989; Hess and Wiegner 1994). Such pristine particles are found in the Antarctic atmosphere (Tape 1994), but elsewhere more complex particles are common. Later, the single-scattering characteristics associated with complex habits, such as bullet rosettes, hollow columns, polycrystals, aggregates, and clusters (or aggregates) of bullet rosettes, were investigated using the ray-tracing technique (e.g., Macke 1993; Macke et al. 1996b; Takano and Liou 1995; Iaquinta et al. 1995; Yang and Liou 1998; Zhang et al. 2004; Um and McFarquhar 2007). The ray-tracing technique in combination with the Monte Carlo method has been applied to the computation of the scattering properties of inhomogeneous ice particles, that is, ice particles with the internal in-

clusion of air bubbles (Macke et al. 1996a; C.-Labonnote et al. 2000, 2001). Furthermore, improved algorithms for the geometric optics method have been developed for light-scattering calculations involving nonspherical ice particles (Muinonen 1989; Yang and Liou 1996b). The results from these efforts over the past two decades have been applied to the parameterization of the radiative properties of ice clouds (Fu et al. 1998; McFarquhar et al. 2002; Key et al. 2002), the remote sensing of ice clouds (Minnis et al. 1993a,b; King et al. 2004; Baum et al. 2005a,b), and the interpretation of the spectral signature of cirrus clouds (Wendisch et al. 2007).

In this study we investigate the scattering and polarization characteristics of hollow bullet rosette ice particles. Bullet rosettes are frequently observed in mid-latitude ice clouds (Heymsfield et al. 2002), and are also common in snowfall on the Antarctic Plateau (Walden et al. 2003). The bullet elements of these particles usually have hollow ends, as evident from *in situ* measurements recently reported by Schmitt and Heymsfield (2007). Based on the modification of a ray-tracing computational model developed by Iaquinta et al. (1995), Schmitt et al. (2006) investigated the scattering properties of hollow bullet rosettes, but did not report the complete phase matrix. As polarimetric quantities (e.g., the backscattering depolarization ratio) contain important information about cloud optical and microphysical properties (Yang et al. 2003; Hu et al. 2007) that can be exploited in remote sensing studies, it is necessary to understand the complete polarization configuration associated with the scattering of light by bullet rosettes. The hollowing of the bullets also has consequences for the absorption of near-infrared solar radiation by ice clouds; the hollowing decreases the mass-to-surface-area ratio of the particles, a quantity that is proportional to the mean absorption pathlength for the radiation transmitted through the bullet rosette.

As a follow-up of the study by Schmitt et al. (2006), we report the complete phase matrix of hollow bullet rosettes. Unlike Schmitt et al. (2006), who assume that the tip of a bullet element has three faces, we define a bullet tip as a pyramid that has six triangular faces, a geometry that is more in line with observations. This paper is organized as follows. In section 2, we define the geometries for bullet rosettes that have various numbers of bullets. We also illustrate the dependence of the projected area of a bullet rosette, expressed as a function of the particle's maximum dimension, aspect ratio, and number of bullets. In section 3, we briefly describe the scattering computational model used in this study. In section 4, we discuss the computed results for the phase matrix, backscattering depolarization ratio, and

asymmetry factor of hollow bullet rosettes. In section 4, we also illustrate the optical effects that result from the inclusion of hollow structures in the individual bullets, and their influence on the prediction of ice cloud microphysical and optical properties (particle effective size and optical thickness, in particular). The conclusions of this study are given in section 5.

2. Geometry of hollow bullet rosettes

A recent analysis of balloonborne replicator data acquired during three ascents through midlatitude cirrus clouds shows that 50%–80% of bullets are not solid (Schmitt and Heymsfield 2007). High-resolution photographs of the particle habits have been obtained by collecting ice particles naturally falling to the surface on the Antarctic Plateau. Walden et al. (2003) analyzed 84 photographs taken on 84 days during the winter of 1992. Figure 1 is typical of the particles falling during snowfall from nimbostratus clouds. In all the bullet clusters photographed during the winter, the bullets were hollow (Table 4 of Walden et al. 2003). Hollow bullet rosettes are more likely to form at rapid particle growth rates and levels of supersaturation similar to the conditions that lead to the development of hollow columns. Since they formed at the low temperatures in the stable atmosphere of the Antarctic Plateau, hollow bullet rosettes could be expected in bullet clusters elsewhere, as Schmitt and Heymsfield (2007) found. The interior walls of the hollow portion of the rosettes are often corrugated as seen in Fig. 1, but in this paper we consider only flat-walled hollow structures. For the particles shown in Fig. 1, the corresponding size parameters at visible and near-infrared wavelengths are clearly within the geometric optics regime.

Figure 2 shows the geometry of a single bullet branch as defined in this study. Note that the present bullet geometry is different from that defined by Iaquinta et al. (1995) and Schmitt et al. (2006), who assumed a trilateral pyramidal tip for a bullet branch. In our definition, the length of the columnar part, tip length, hollow depth, and width of the bullet are indicated by L , t , H , and $2a$, respectively. The angle between the axis of symmetry and the pyramidal faces is indicated by α following the notation used by Greenler (1980). Note that only two parameters among t , a , and α are independent. Specifically, we have the following relationship:

$$\tan \alpha = \frac{\sqrt{3}a}{2t} \tag{1}$$

Historically, the value of α was suggested to be either 25° or 28° in the atmospheric optics literature (e.g., Besson 1923). However, Goldie et al. (1976) argued



FIG. 1. Photomicrograph of snow particles falling at the South Pole Station, 18 Aug 1992, at ambient temperature -54°C . The scale bar is 1 mm. A glass slide was set out on the roof of a building daily during winter to collect falling snow and then was photographed through a microscope. This photograph of bullet rosettes is typical of “snow grain” precipitation. It is evident that the bullets contain long hollow structures. (Photograph by S. Warren.)

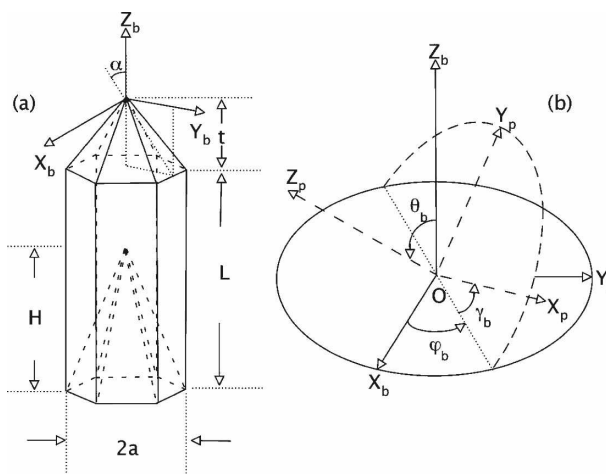


FIG. 2. (a) Geometry of a single bullet with a hollow structure. (b) Transformation between two coordinate systems: the particle system ($O X_p Y_p Z_p$) fixed to a bullet rosette and a coordinate system ($O X_b Y_b Z_b$) fixed to an individual bullet branch.

that $\alpha = 28^\circ$ was required to explain an unusual halo display observed over England. Furthermore, $\alpha = 28^\circ$ leads to a value of 31.5° for the angle between the bullet symmetry axis and the edges of the pyramidal faces, which is consistent with that observed for some bullet ice particles (Tape and Moilanen 2006). For this reason, we assume α to be 28° , and note that this value was also used by Um and McFarquhar (2007).

The geometry of single bullet branch is defined in a coordinate system fixed to the bullet, that is, $OX_bY_bZ_b$ in Fig. 2a. A particle coordinate system, $OX_pY_pZ_p$, is employed to define the geometry of the rosette. The position of a bullet branch in $OX_pY_pZ_p$ is specified by three Euler angles φ_b , θ_b , and γ_b shown in Fig. 2b. The rotational transformation between the two coordinate systems is given as follows:

$$\begin{aligned} \begin{pmatrix} x_p \\ y_p \\ z_p \end{pmatrix} &= \begin{bmatrix} \cos\gamma_b & \sin\gamma_b & 0 \\ -\sin\gamma_b & \cos\gamma_b & 0 \\ 0 & 0 & 1 \end{bmatrix} \begin{bmatrix} 1 & 0 & 0 \\ 0 & \cos\theta_b & \sin\theta_b \\ 0 & -\sin\theta_b & \cos\theta_b \end{bmatrix} \begin{bmatrix} \cos\varphi_b & \sin\varphi_b & 0 \\ -\sin\varphi_b & \cos\varphi_b & 0 \\ 0 & 0 & 1 \end{bmatrix} \begin{pmatrix} x_b \\ y_b \\ z_b \end{pmatrix} \\ &= \begin{bmatrix} \cos\varphi_b \cos\gamma_b - \sin\varphi_b \cos\theta_b \sin\gamma_b & \sin\varphi_b \cos\gamma_b + \cos\varphi_b \cos\theta_b \sin\gamma_b & \sin\theta_b \sin\gamma_b \\ -\cos\varphi_b \sin\gamma_b - \sin\varphi_b \cos\theta_b \cos\gamma_b & -\sin\varphi_b \sin\gamma_b + \cos\varphi_b \cos\theta_b \cos\gamma_b & \sin\theta_b \cos\gamma_b \\ \sin\theta_b \sin\varphi_b & -\sin\theta_b \cos\varphi_b & \cos\theta_b \end{bmatrix} \begin{pmatrix} x_b \\ y_b \\ z_b \end{pmatrix}, \quad (2) \end{aligned}$$

where (x_b, y_b, z_b) indicate the coordinates in $OX_bY_bZ_b$, whereas (x_p, y_p, z_p) are the corresponding coordinates in $OX_pY_pZ_p$.

Figure 3 shows representations of a single hollow bullet and various hollow bullet rosettes consisting of between 2 and 12 hollow bullet branches. Different values have been reported in the literature for the mean number of bullet branches, $\langle n_b \rangle$, for bullet rosettes observed in cirrus clouds. For example, an analysis of 869 ice particle images by Heymsfield et al. (2002) that were acquired over the U.S. Department of Energy–Atmospheric Radiation Measurement Program (ARM) site in Oklahoma on 9 March 2000 shows a value of $\langle n_b \rangle = 5.8 \pm 0.6$, whereas the number of bullet branches per rosette ranges from 2 to 12. From an analysis of the ice particle replicator data (Arnott et al. 1994) acquired near Coffeyville, Kansas, during the First International Satellite Cloud Climatology Project (ISCCP) Regional Experiment (FIRE-I) held in 1991, Mitchell and Arnott (1994) estimated that the average number of branches per rosette is approximately 11. The Antarctic rosettes had 1–9 branches (except for one outlier with 16), averaging 4 per particle (Walden et al. 2003, Table 2; V. P. Walden 2004, personal communication). In many reported studies, with the exception of Iaquinta et al. (1995), 4- or 6-branched bullet rosettes are usually assumed (Takano and Liou 1995; Yang and Liou 1998). Um and McFarquhar (2007) also used 4-branched and 6-branched bullet rosettes to define aggregates of bullet rosettes. While Iaquinta et al. (1995) investigated the effect of branch number on the single-scattering prop-

erties of solid bullet rosettes, a similar sensitivity study should be carried out in the case of hollow bullet rosettes.

The aspect ratio (i.e., the ratio of width to length) of a bullet branch is an important morphological parameter that influences the optical properties of the rosette. An empirical relationship for bullet rosette aspect ratios was developed by Mitchell and Arnott (1994) as follows:

$$a/L = 1.16L^{-0.37} \quad \text{for } 100 \mu\text{m} \leq L \leq 500 \mu\text{m}. \quad (3)$$

The units for the expression in Eq. (3) are in micrometers. Note that the units in the original expression given by Mitchell and Arnott (1994) are in centimeters. A recent study by Um and McFarquhar (2007), who assumed 6-branched bullet rosettes to fit the aspect ratio data associated with 89 ice particle images, reports the following aspect ratio relation:

$$a/L = 3.57L^{-0.545} \quad \text{for } 100 \mu\text{m} \leq L \leq 600 \mu\text{m}. \quad (4)$$

We define the maximum dimension of a bullet rosette in terms of the diameter of its minimum circumscribing sphere following Heymsfield et al. (2002). Thus, from the geometry shown in Fig. 2, the maximum

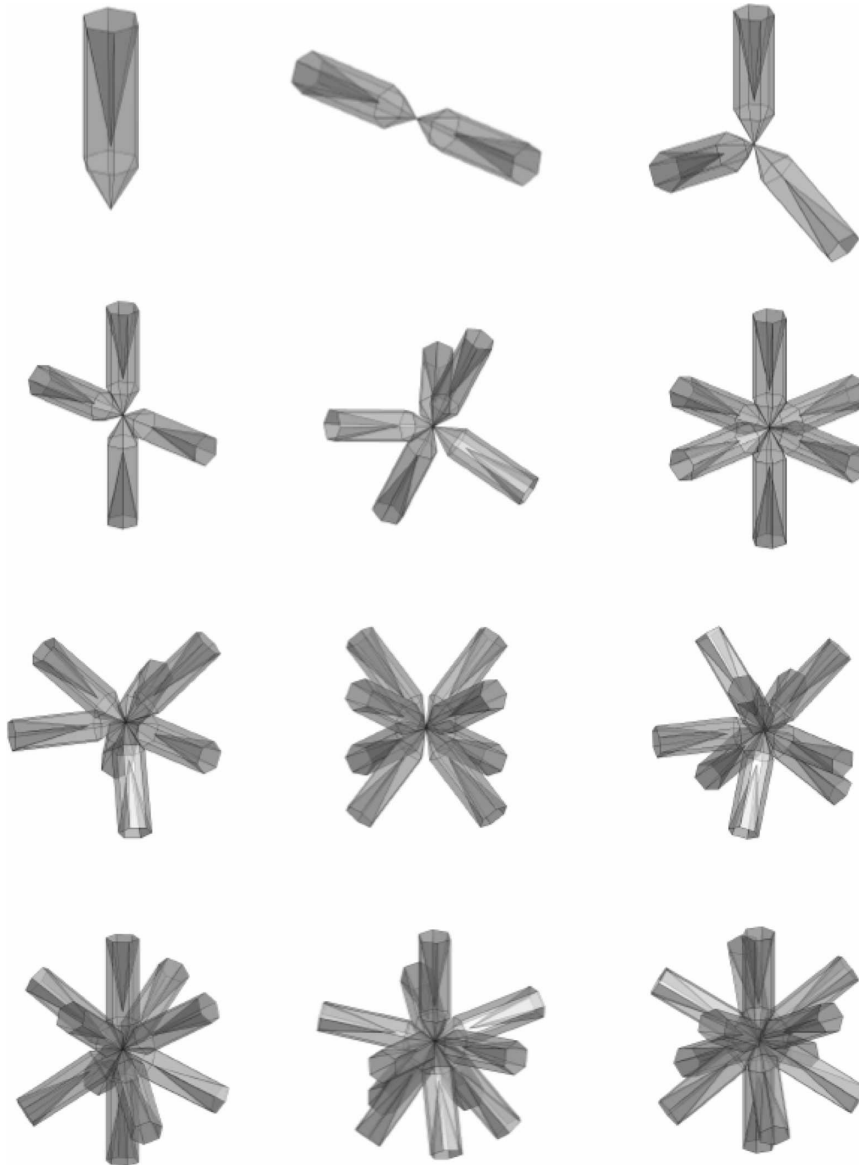


FIG. 3. The geometries of (top left) a single hollow bullet as well as for hollow bullet rosettes with 2–12 branches.

dimension of a bullet rosette with two or more branches is given by

$$D = 2\sqrt{(t + L)^2 + a^2}. \quad (5)$$

The top panel of Fig. 4 compares the aspect ratio expressions given by Eqs. (3) and (4). It is evident that the bullet branches specified by Eq. (3) are thinner than their counterparts based on Eq. (4). The differences are especially pronounced for moderate particle sizes (i.e., $L \sim 50 \mu\text{m}$). For large ($L > 400 \mu\text{m}$) bullet rosettes, the two relations converge. The bottom panel of Fig. 4

shows two relationships between L and D that are calculated using Eqs. (3) and (4). The L – D relationships are similar because the small aspect ratio of the bullets means that D is insensitive to a . In particular, the L – D relationships derived from Eqs. (3) and (4) are essentially the same when L is larger than approximately $1200 \mu\text{m}$. In this limit, Eq. (5) approximates to $D \approx 2(t + L)$.

Figure 5 shows the projected areas calculated from Eqs. (3) and (4) as a function of the maximum dimension for bullet rosettes that are assumed to have 6 or 11 branches. For comparison, the measurement data are

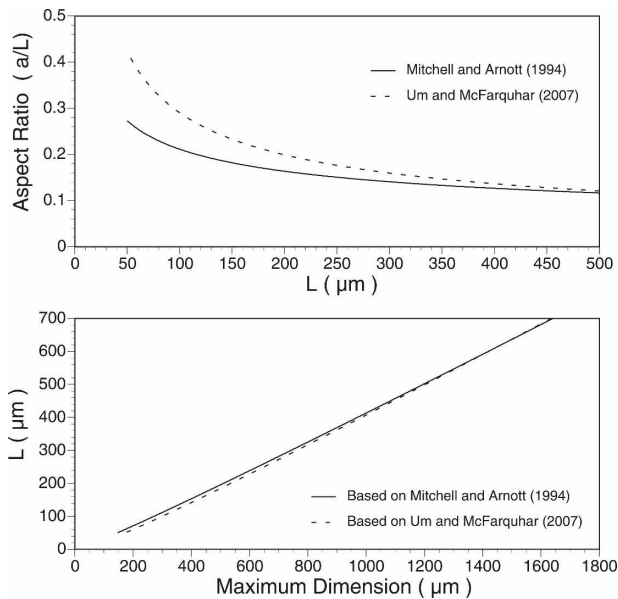


FIG. 4. (top) The aspect ratio relations reported by Mitchell and Arnott (1994) and Um and McFarquhar (2007), corresponding to Eq. (3) and Eq. (4), respectively. (bottom) Relationships between L (the length of columnar part of a bullet branch) and D (the maximum particle dimension) derived from the two aspect ratio relations showed in the top panel.

shown from Arnott et al. (1994). Note that each measurement data point shown in Fig. 5 represents an average of a number of ice particle images (see Arnott et al. 1994 for details). In the case of 11-branched bullet rosettes, the projected areas computed from either Eq. (3) or Eq. (4) are substantially overestimated in comparison with the measurements when D is larger than $400 \mu\text{m}$. The overestimation is more pronounced in the case of the results based on Eq. (4). However, if 6 branches are assumed for bullet rosettes, the projected areas simulated on the basis of the aspect ratio relationship defined in Eq. (4) agree better with the observations than those based on Eq. (3). Furthermore, the limited datasets in Fig. 5 suggest that large bullet rosette ice particles have fewer branches than small particles.

3. Scattering computational model

Observations reported by Arnott et al. (1994) and Mitchell and Arnott (1994) show that bullet rosettes are generally larger than $200 \mu\text{m}$. Thus, the optical properties of these particles cannot be derived from rigorous numerical approaches such as the discrete dipole approximation (DDA; Draine and Flatau 1994) and the finite-difference time domain (FDTD) method (Yee 1966; Taflove 1995; Yang and Liou 1996a; Sun et al.

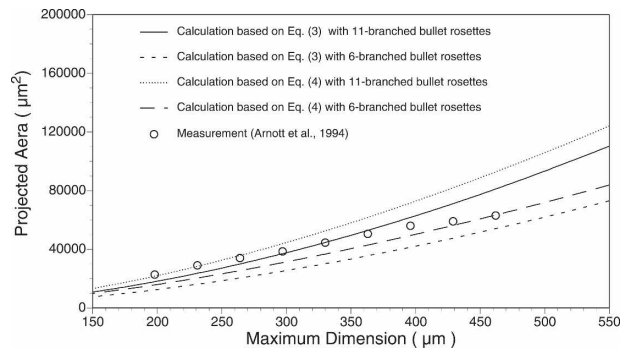


FIG. 5. Measured and projected area as function of particle maximum dimension, which is calculated from the two aspect ratio relations shown in Fig. 4 for 11- and 6-branched hollow bullet rosettes.

1999). The large size parameters prevent the application of these methods because of their tremendous demand on computer CPU time and memory. Note that comprehensive reviews of various rigorous and approximate methods for light-scattering computations can be found in Mishchenko et al. (2000) and Kahnert (2003). When size parameters are larger than approximately 80, the conventional geometric optics method, also called the ray-tracing method, can be applied to the computation of the single-scattering properties of dielectric particles (Macke et al. 1995; Mishchenko and Macke 1999; Wielaard et al. 1997).

For our calculations, we use an improved geometric optics method (IGOM) developed by Yang and Liou (1996b) to compute the single-scattering properties of hollow bullet rosettes. Unlike the conventional ray-tracing technique, IGOM does not separate the extinction of the incident radiation into equal contributions from diffraction and reflected-refracted Fresnelian rays. In IGOM, the ray-tracing calculation is carried out to compute the near field on the particle surface, which is subsequently mapped to the far field using a rigorous electromagnetic relationship that relates the near field to the far field. The concept of mapping the near field to the corresponding far field was first reported by Muinonen (1989). A previous study compared the IGOM results with the FDTD solutions for light scattering by small ice particles (Yang and Liou 1996b). For computational efficiency, we employ the simplified IGOM algorithm (Yang and Liou 1996b) that remaps the phase matrix computed from the conventional ray-tracing technique by taking into account the ray spreading effect. The technical details of the simplified IGOM are tedious and are reported by Yang and Liou (1996b). Most recently, Yang et al. (2007) showed that the simplified IGOM offers a reasonable approximation of the phase matrix of randomly oriented spheroids with size

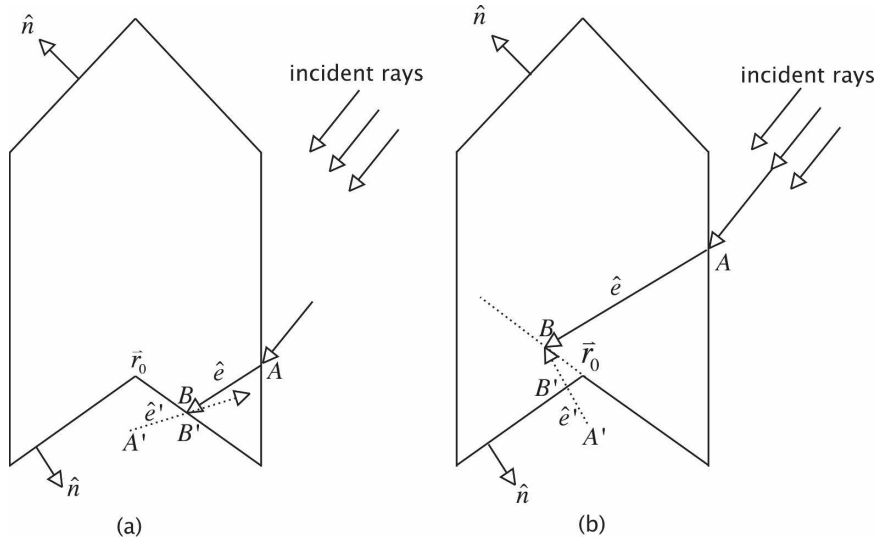


FIG. 6. A schematic that illustrates whether an incident ray impinges on the hollow intrusion in an individual bullet: (a) a ray that impinges upon the hollow intrusion; (b) a ray that does not impinge upon the hollow intrusion.

parameters larger than 30–40, as compared with that computed from the T-matrix method (Mishchenko and Travis 1994). As the size parameters involved in this study are on the order of 1000, the simplified IGOM is applicable. For these large size parameters, the solutions from the simplified IGOM are essentially the same as those from the conventional ray-tracing technique; the scattering peaks corresponding to halos are especially pronounced.

The most tedious step in computing the single-scattering properties of hollow bullet rosettes from the IGOM method may be the ray-tracing calculation. Although numerous algorithms can be used to trace the propagation of an incident ray on the basis of Snell’s law, we found that the algorithm illustrated in Fig. 6 is computationally straightforward and efficient. The example illustrated in Fig. 6 shows how to determine the next impinging point of a ray refracted into a hollow bullet branch. As shown in Fig. 6a, the initial incident point of a certain ray is A whose position vector is denoted by \mathbf{r}_A (not shown in the diagram). A unit vector $\hat{\mathbf{n}}$ denotes the outward normal direction for a particle face. The position vector of the apex of the pyramidal tip of the hollow structure is denoted by \mathbf{r}_0 . To determine the next impinging point of the refracted ray, it is necessary to determine whether the ray intercepts with the pyramidal hollow end. A necessary condition for the interception of the ray by a face of the pyramidal hollow section at the end of the bullet is as follows:

$$\hat{\mathbf{e}} \cdot \hat{\mathbf{n}} > 0. \tag{6}$$

If the condition in Eq. (6) is satisfied, an impinging point denoted as point B or by a position vector \mathbf{r}_B (not shown in the diagram) on this pyramidal face can be determined as follows:

$$\mathbf{r}_B = \mathbf{r}_A + l\hat{\mathbf{e}}, \quad \text{where} \tag{7a}$$

$$l = \frac{(\mathbf{r}_0 - \mathbf{r}_A) \cdot \hat{\mathbf{n}}}{\hat{\mathbf{n}} \cdot \hat{\mathbf{e}}}. \tag{7b}$$

After point B is determined, a new unit vector $\hat{\mathbf{e}}'$ can be defined as follows:

$$\hat{\mathbf{e}}' = \frac{\mathbf{r}_B - \mathbf{r}_{A'}}{|\mathbf{r}_B - \mathbf{r}_{A'}|}, \tag{8}$$

where $\mathbf{r}_{A'}$ denotes the position vector of the center (point A' in the diagram) of the hollow end. Among all the faces that satisfy $\hat{\mathbf{e}}' \cdot \hat{\mathbf{n}} < 0$ there is one face that has the shortest distance from point A' . Let the intercepting point on this face be B' , as shown in Fig. 6. If points B and B' are on the same pyramidal face such as in the case shown in Fig. 6a, then the ray impinges on the hollow end at point B . Unlike the case illustrated in Fig. 6a, point B' and B in Fig. 6b are not coincident, and thus the ray does not intercept the hollow end. In this case, we can find the impinging point by considering those faces other than the hollow faces with $\hat{\mathbf{e}} \cdot \hat{\mathbf{n}} > 0$ and search for the one

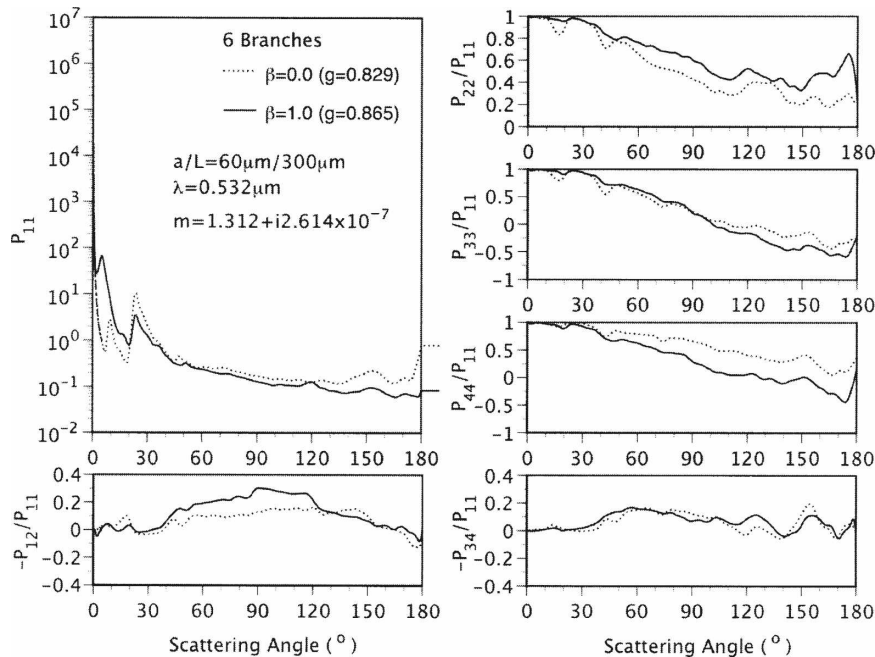


FIG. 7. Comparison of the phase matrices of solid and hollow bullet rosette ice particles at a wavelength of $0.532 \mu\text{m}$. Note that β is the ratio of the length of the hollowness to the length of the bullet branch. Here $\beta = 0.0$ indicates that the bullet branch is solid, and $\beta = 1.0$ indicates that the depth of the hollow structure is equal to the length of the branch.

that has the shortest distance from point *A* as determined by Eqs. (7a) and (7b). Note that Eqs. (6)–(8) do not depend on a specific coordinate system. Thus, this algorithm can be easily implemented in either a laboratory coordinate system or the particle coordinate system. Furthermore, we use the approach reported in Zhang et al. (2004) to determine whether an outgoing ray is blocked by a bullet branch. If the ray is not blocked, the ray will be considered as a scattered ray; otherwise, the reflection–refraction event is considered with respect to that bullet branch.

4. Results and discussion

Figure 7 shows the comparison of the phase matrices of 6-branched solid and hollow bullet rosettes for an incident wavelength of $0.532 \mu\text{m}$. This wavelength could be considered as representative of a lidar measurement such as from the Cloud-Aerosol Lidar with Orthogonal Polarization (CALIOP) on the Cloud-Aerosol Lidar and Infrared Pathfinder Satellite Observation (CALIPSO). CALIOP takes measurements at 0.532 and $1.064 \mu\text{m}$ (Winker et al. 2007).

All ice particles are assumed to be randomly oriented

in space. The parameter β in Fig. 7 is defined as follows:

$$\beta = H/(t + L). \quad (9)$$

Thus, $\beta = 0$ indicates a solid bullet rosette whereas $\beta = 1$ represents the maximum hollow structure depth. It is evident from Fig. 7 that the 22° halo peak observed in the phase function is substantially reduced for hollow bullet rosettes because the hollow structures alter the paths of a substantial number of rays associated with the 22° minimum deviation angle responsible for this scattering peak.

The most significant effect of the hollow structures in the bullet branches is the reduction of the phase function values at scattering angles near the backscattering direction. Specifically, the backscattered intensity associated with hollow bullet rosettes is approximately 10 times smaller than its counterpart in the solid case. This may have an implication for active remote sensing of ice clouds.

Another effect of including hollow structures at the ends of the bullets is to increase the magnitude of the phase function at scattering angles between $\sim 1^\circ$ and 20° . The behavior of the other phase matrix elements is generally similar for solid and hollow bullet rosettes. However, at scattering angles larger than approximately 50° , the P_{22}/P_{11} and P_{44}/P_{11} values are quite

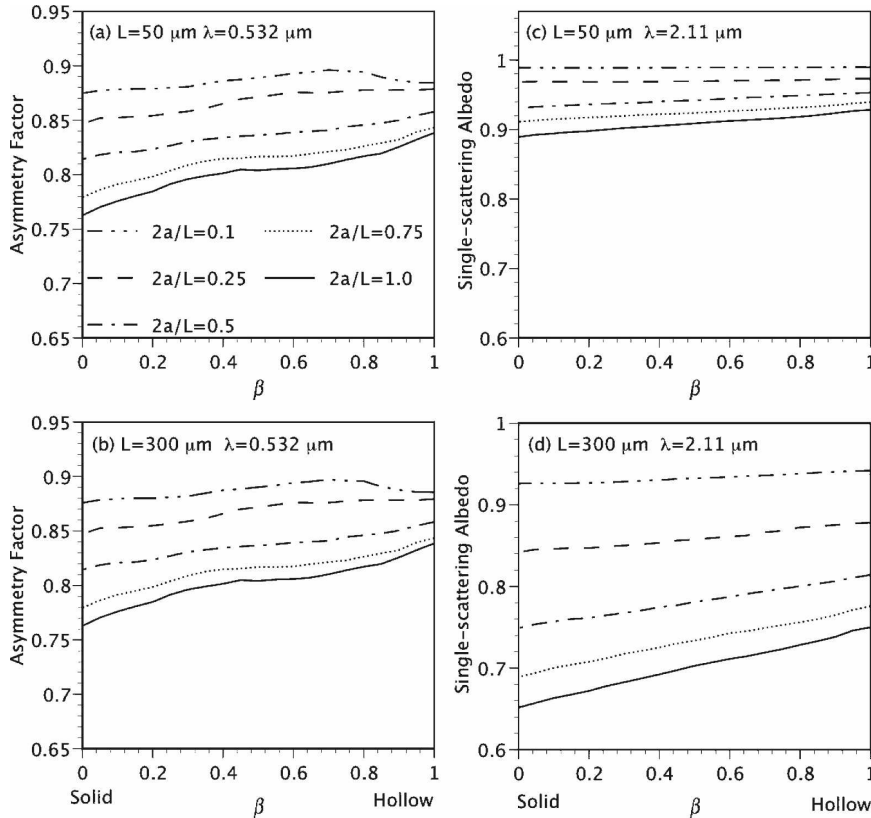


FIG. 8. (a), (b) Variation of the asymmetry factor with the depth of the hollow structure for various aspect ratios at a wavelength of $0.532 \mu\text{m}$. (c), (d) Variation of the single-scattering albedo with the depth of the hollow structure for various aspect ratios at a wavelength of $2.11 \mu\text{m}$.

different for hollow and solid bullet rosettes. For $-P_{12}/P_{11}$, often referred to as the degree of linear polarization, the differences between the solutions for the hollow and solid bullet rosettes are observed primarily in a region of approximately 40° – 120° as well as in the 22° halo region.

We also compute the fraction of the scattered energy within an angular region of scattering angles smaller than 0.1° , which is associated with transmitted rays but excludes the diffraction contribution. This fraction (f_δ) is equivalent to the delta transmission discussed by Takano and Liou (1989) and Mishchenko and Macke (1998). The total scattering phase function that includes this effect can be expressed as follows:

$$P_{11,r}(\theta) \approx 2f_\delta\delta(\cos\theta - 1) + (1 - f_\delta)P_{11}(\theta), \quad (10)$$

where δ is the Dirac delta function, and $P_{11}(\theta)$ is the continuous component of the phase function shown in Fig. 7. The values of f_δ are 0.1222 and 0.003 37 for the solid and hollow bullet rosettes, respectively. The sig-

nificant reduction of f_δ for the hollow bullet rosettes occurs because the hollow structures alter the ray paths for many rays that would otherwise transmit directly through two parallel faces if the bullets were solid.

The hollow structures in the bullets increase the scattering phase function values within the forward scattering angle region from 1° to 20° , a conclusion similar to that of Schmitt et al. (2006), but decrease values at side- and backscattering angles of 60° – 180° . As a result, the presence of the hollow structures tends to increase the asymmetry factor. The values of the asymmetry factor associated with hollow and solid bullet rosettes whose phase functions are shown in Fig. 7 are 0.865 and 0.829, respectively.

Figures 8a,b show the asymmetry factor values for various aspect ratios and hollow depths for bullet rosettes with $L = 50$ and $300 \mu\text{m}$. For a given β and L , the asymmetry factor decreases with increasing aspect ratio in a range of $2a/L = 0.1 - 1$. This is consistent with a phenomenon noticed by Grenfell et al. (2005) and Fu (2007), who found a minimum in the asymmetry factor when $2a/L \approx 1$ (i.e., compact ice particles) for the case

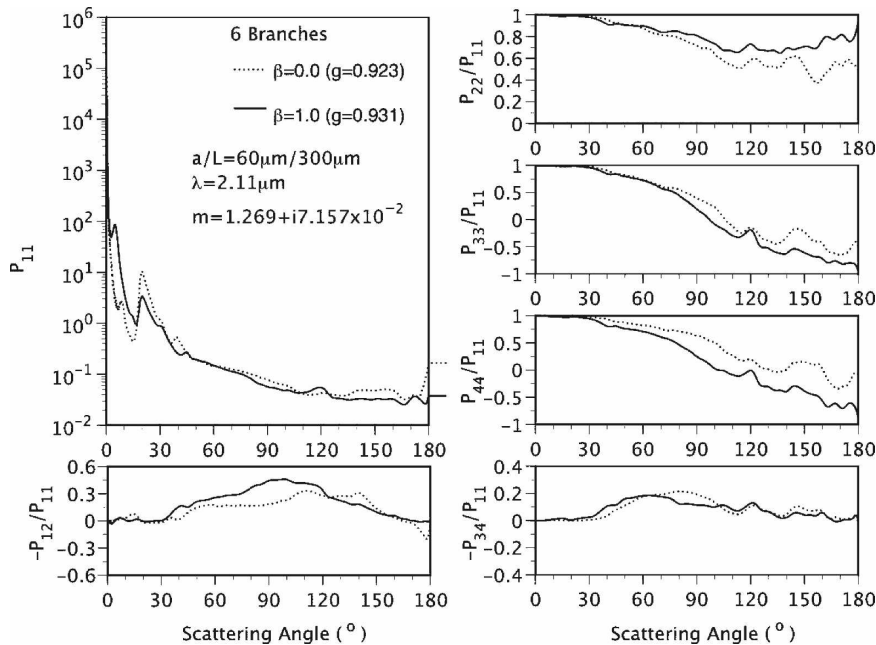


FIG. 9. As in Fig. 7, but at a wavelength of 2.11 μm .

of hexagonal pristine ice particles. The results in Figs. 8a,b for hollow bullet rosettes demonstrate that the asymmetry factor increases with an increase of the hollow structure depth, except in the case of $2a/L = 0.1$ and $\beta > 0.8$. Schmitt et al. (2006) also showed that the asymmetry factor is quite sensitive to the presence of the hollow structures on the bullets as well as the aspect ratios of bullet branches. Specifically, Fig. 4 in Schmitt et al. (2006) shows g increasing with hollowness for $2a/L = 0.5 - 1$, but not for longer and thinner bullets.

Another outstanding effect of the hollow bullets is to increase the single-scattering albedo. Figures 8c,d show the single-scattering albedos of hollow rosettes with various aspect ratios as a function of β at a near-infrared wavelength of 2.11 μm for particle sizes of 50 and 300 μm , respectively. The single-scattering albedo generally increases with β ; that is, the absorption of a rosette decreases with the increase of the hollow structure depth. This occurs because the hollow structures at the ends of bullet branches reduce the mass-to-surface-area ratio of the particle, which in turn reduce the mean absorption pathlength for the rays transmitted through the particle.

A commonly used approach to retrieve cloud microphysical and optical properties (specifically, optical thickness and effective particle size) from reflected sunlight during daytime is a bispectral method (Nakajima and King 1990; Platnick et al. 2003) that is based on

radiometric measurements at a nonabsorbing band (e.g., 0.66- or 0.86- μm band) and a slightly absorbing band (e.g., 2.11- or 1.64- μm band). The absorbing band provides the information content for retrieving the effective particle size. For this reason, we also investigate the optical properties of hollow bullet rosettes at a near-infrared wavelength. Figure 9 shows the phase matrix computed for an incident wavelength of 2.11 μm . The particle geometry for Fig. 9 is the same as that for Fig. 7. The effect of the hollow bullet structures on the phase matrix for the near-infrared wavelength is similar, but not as pronounced, as that for a visible wavelength.

In Figs. 7, 8, and 9, the angles between the bullet branches of a 6-branched bullet rosette ice particle are assumed to be 90°. Observations show that the frequency distribution of angles between two bullet branches peaks primarily at 70°, although 90° has also been observed (Kobayashi et al. 1976; Takano and Liou 1995; Iaquinta et al. 1995, and references cited therein). Figure 10 shows the phase functions of 4-branched hollow bullet rosettes with $\beta = 0.5$. The angle between any two branches is specified as 70° (or its supplement angle, 110°) or 90°. Evidently, a choice of 70° or 90° has little effect on the phase matrix.

Figure 11 shows the phase matrices of 1-, 6-, and 12-branched hollow bullet rosettes at a wavelength of 0.532 μm . The hollow structure depth is $\beta = 1$. The differences are small in the optical properties of these

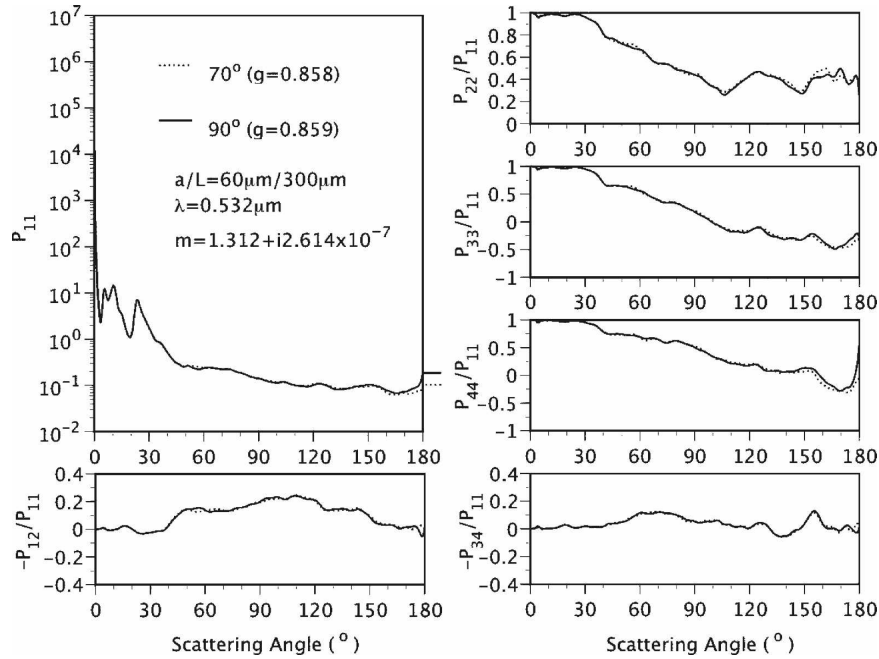


FIG. 10. Comparison of phase matrices of 4-branched hollow bullet rosette ice particles with angles between bullet branches of 70° and 90°. The depth of the hollow depth is specified as $\beta = 0.5$.

three particles. Iaquina et al. (1995) previously noted that the scattering properties of bullet rosettes depend only weakly on the number of bullet branches. At scattering angles larger than 90°, the phase function values

tend to increase slightly with an increase in the number of bullets. The effect of the number of bullet branches on the other phase matrix elements is also small except for P_{22}/P_{11} at scattering angles larger than 150°. A scat-

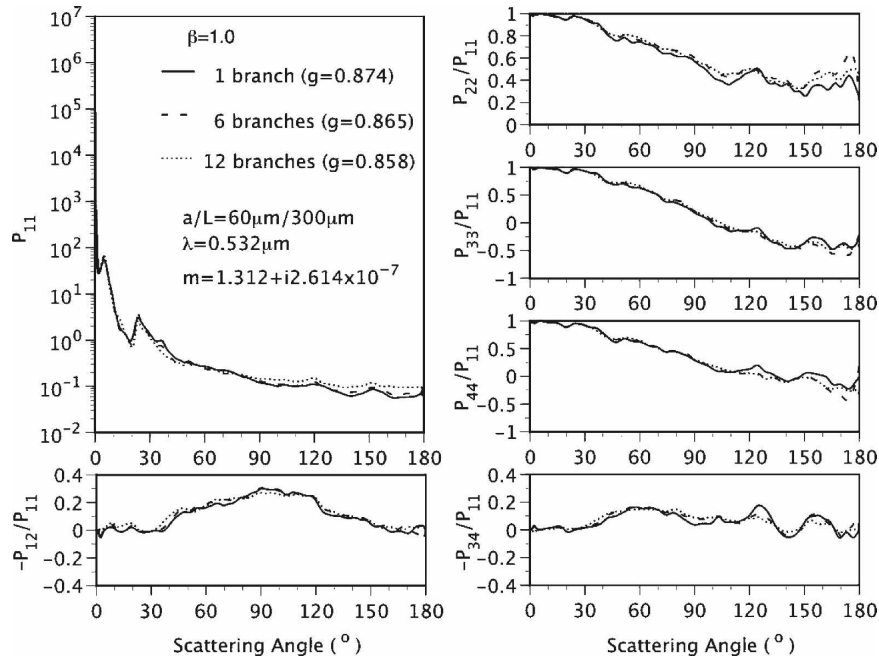


FIG. 11. Comparison of phase matrices of 1-, 6-, and 12-branched hollow bullet rosette ice particles.

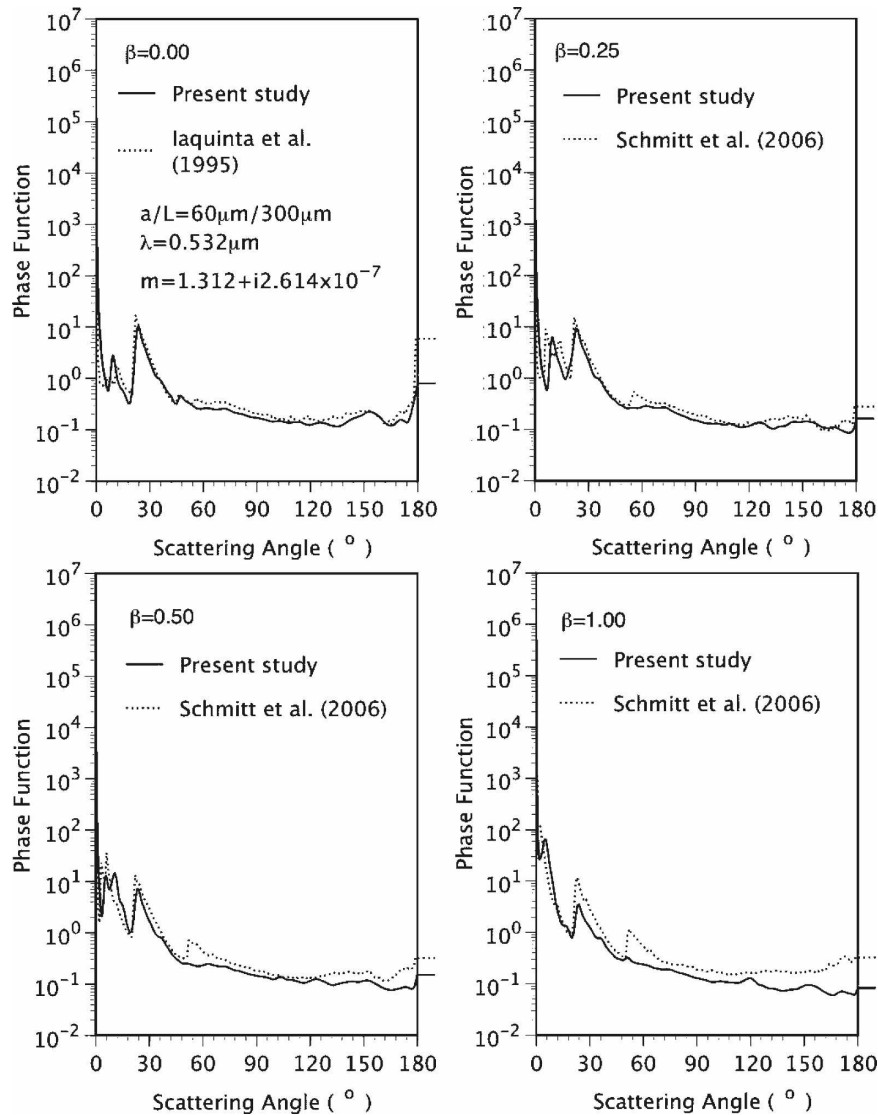


FIG. 12. Comparison of the phase functions computed from the present method and the model reported by Iaquinta et al. (1995) for solid rosettes ($\beta = 0.0$) and the model by Schmitt et al. (2006) for hollow rosettes ($\beta = 0.25, 0.50$, and 1.0).

tering peak was observed at approximately 55° in the phase function of 6-branched bullet rosettes as computed by Schmitt et al. (2006; see the lower panel in their Fig. 3). However, this peak is not observed in the present study. This may be a result of the different bullet geometries assumed in these two studies and warrants further investigation.

Figure 12 shows the phase functions computed from the present model in comparison with those computed from the ray-tracing models reported by Iaquinta et al. (1995) and Schmitt et al. (2006). The model reported in Iaquinta et al. (1995) was designed for solid bullet rosettes and Schmitt et al. (2006) extended this model to

hollow rosettes. In the case of solid bullet rosettes (i.e., $\beta = 0$), it is evident from Fig. 12 that our results generally agree well with the solution from the model developed by Iaquinta et al. (1995), except that our phase function values are lower at a scattering angle of 180° (i.e., backscattering). In the case of hollow bullet rosettes, there are significant differences between the present results and those from Schmitt et al. (2006), particularly for $\beta = 0.5$ and 1.0 . Additionally, the phase functions computed from the present method have lower values for scattering angles larger than approximately 40° , and a scattering peak at $\sim 55^\circ$ is not observed.

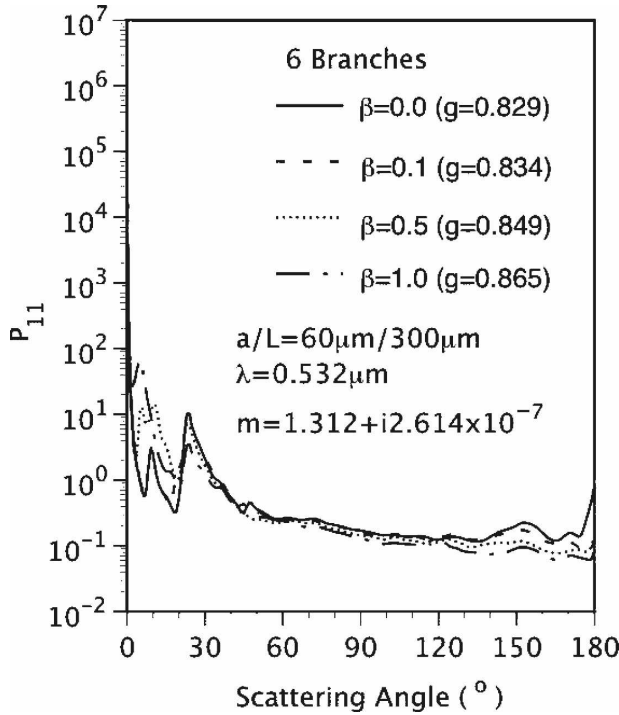


FIG. 13. Comparison of the phase functions of randomly oriented hollow bullet rosette ice crystals with various hollow structure depths. The solid line corresponding to $\beta = 0.0$ indicates the phase function for randomly oriented solid bullet rosette ice crystals.

Figure 13 shows the phase functions for solid ($\beta = 0$) and hollow ($\beta = 0.1, 0.5,$ and 1) bullet rosettes. The backscattered intensity decreases with the increase of the hollow structure depth. In the case of $\beta = 1$, the scattering maximum at 154° is not observed. The locations of the scattering peaks at scattering angles less than 22° , which are associated with rays that interact with the pyramidal tips of the bullet branches, are sensitive to the hollow structure depth. The scattering angle where the scattering peak is observed decreases with an increase of the hollow structure depth.

For remote sensing applications, the bulk scattering properties of ice clouds are needed as functions of the effective particle size. These properties are obtained by averaging the single-scattering properties of ice particles over the particle size distributions (PSDs) as follows:

$$\langle Q_e \rangle = \frac{\int_{D_{\min}}^{D_{\max}} Q_e(D)A(D)n(D) dD}{\int_{D_{\min}}^{D_{\max}} A(D)n(D) dD}, \quad (11)$$

$$\langle \varpi \rangle = \frac{\int_{D_{\min}}^{D_{\max}} \varpi(D)Q_e(D)A(D)n(D) dD}{\int_{D_{\min}}^{D_{\max}} Q_e(D)A(D)n(D) dD}, \quad (12)$$

$$\langle g \rangle = \frac{\int_{D_{\min}}^{D_{\max}} g(D)\varpi(D)Q_e(D)A(D)n(D) dD}{\int_{D_{\min}}^{D_{\max}} \varpi(D)Q_e(D)A(D)n(D) dD}, \quad (13)$$

and

$$\langle P \rangle = \frac{\int_{D_{\min}}^{D_{\max}} P(D)\varpi(D)Q_e(D)A(D)n(D) dD}{\int_{D_{\min}}^{D_{\max}} \varpi(D)Q_e(D)A(D)n(D) dD}, \quad (14)$$

where D and A are the maximum dimension and projected area of an ice particle, respectively. Here $n(D)$ specifies the number density of ice particles with the maximum dimension between D and $D + dD$; D_{\min} and D_{\max} are the lower and upper boundary of the PSD; and Q_e , ϖ , g , and P are the extinction efficiency, single-scattering albedo, asymmetry factor, and scattering phase matrix, respectively. The symbol $\langle \rangle$ denotes that the relevant scattering property is averaged for a population of ice particles. The effective particle size in this study is proportional to the volume-to-projected-area ratio as follows (Foot 1988; King et al. 2004):

$$D_e = \frac{3}{2} \frac{\int_{D_{\min}}^{D_{\max}} V(D)n(D) dD}{\int_{D_{\min}}^{D_{\max}} A(D)n(D) dD}, \quad (15)$$

where V is the volume of an ice particle. In this study the volume of a hollow rosette is defined to exclude that associated with the hollow structures. Note that for a monodispersion of solid spheres, D_e is just the diameter of the spheres. The PSDs used in this study are obtained from several major field campaigns of in situ ice cloud observations over the last few decades. The same datasets were also used in the development of ice cloud optical models for the Moderate Resolution Imaging Spectroradiometer (MODIS) operational (collection 5) cloud retrievals. Detailed discussions of the PSD data are provided in Baum et al. (2005a) and the references cited therein.

Figure 14 shows the bulk scattering asymmetry factor for a size distribution of hollow bullet rosettes as a function of D_e at a wavelength of $0.532 \mu\text{m}$. In the

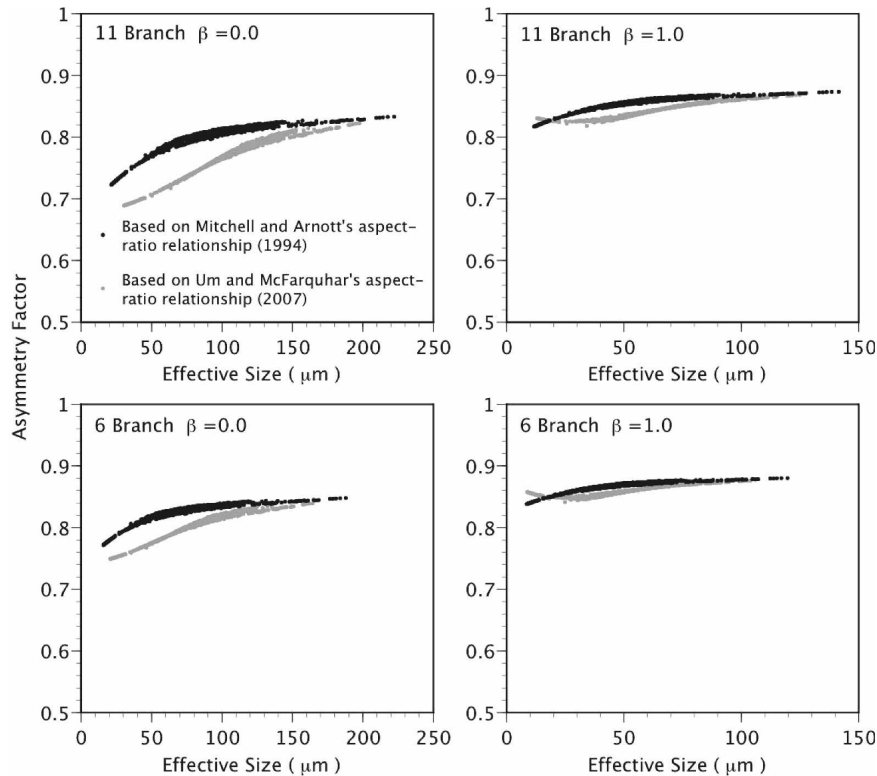


FIG. 14. Bulk asymmetry factor of hollow bullet rosettes—(top) 11 and (bottom) 6 branches—as a function of effective particle size at a wavelength of $0.532 \mu\text{m}$ for (left) $\beta = 0.0$ and (right) $\beta = 1.0$.

calculation, 6 or 11 branches are assumed for bullet rosettes, and the aspect ratio relations reported by Mitchell and Arnott (1994) and Um and McFarquhar (2007) are used. Similar to the case of individual hollow bullet rosette particles, the inclusion of hollow structures substantially increases the asymmetry factor of a population of hollow bullet rosettes, particularly for rosettes with 11 branches. We note that the phase functions shown earlier in Fig. 11 are not sensitive to the number of bullet branches, except in the forward direction where the magnitude of the diffraction contribution is proportional to the particle projected area. In Fig. 11, the phase function is expressed as a function of particle maximum dimension. However, the results shown in Fig. 14 are expressed as functions of the effective particle size. In the calculation involved for Fig. 11, the aspect ratio is specified by Eq. (3) or Eq. (4) for a given maximum dimension. The weighting of the particle in the computation of the effective particle size is different for 11- and 6-branched bullet rosettes. Thus, the asymmetry factor depends both on the number of bullet branches, which is illustrated in Fig. 14, and the effective particle size. The asymmetry factor values calculated on the basis of the aspect ratio reported by

Mitchell and Arnott (1994) monotonically increases with D_e in both the hollow and solid bullet rosette cases. However, if the aspect ratio relationship of Um and McFarquhar (2007) is used, hollow bullet rosettes do not show this monotonic variation for small D_e (10–50 μm). The results shown in Fig. 14 suggest that the asymmetry factor values based on these two aspect ratio relationships are quite different, particularly for solid bullet rosettes with $D_e < 120 \mu\text{m}$.

Figure 15 shows the backscattering linear depolarization ratio (δ) as a function of effective particle size for solid ($\beta = 0$) and hollow ($\beta = 1$) bullet rosettes at a wavelength of $0.532 \mu\text{m}$. The backscattering depolarization ratio is defined as follows:

$$\delta = \frac{\langle P_{11}(180^\circ) \rangle - \langle P_{22}(180^\circ) \rangle}{\langle P_{11}(180^\circ) \rangle + \langle P_{22}(180^\circ) \rangle}. \quad (16)$$

Inspection of Fig. 15 shows that δ of hollow bullet rosettes is substantially smaller than that of solid bullet rosettes. Moreover, the variation of δ as a function of the effective particle size for solid and hollow bullet rosettes is significantly different.

Figure 16 shows the bulk scattering phase functions

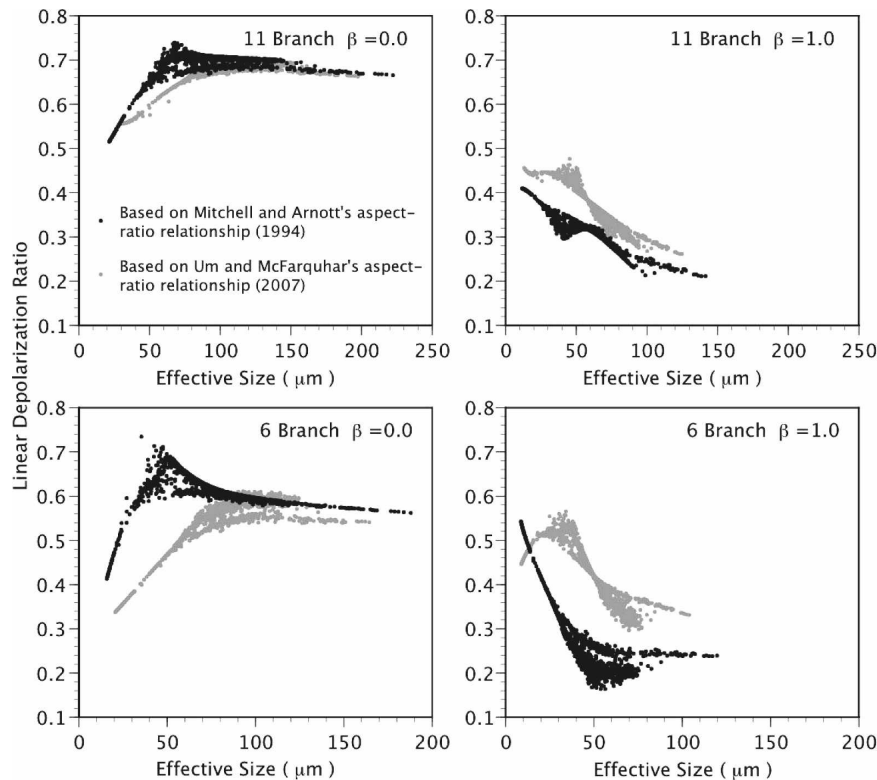


FIG. 15. Single-scattering linear depolarization ratio (δ) at 180° (backscattering) for hollow bullet rosettes—(top) 11 and (bottom) 6 branches—as a function of effective particle size at a wavelength of $0.532 \mu\text{m}$ for (left) $\beta = 0.0$ and (right) $\beta = 1.0$.

of solid and hollow bullet rosettes at wavelengths of 0.86 and $2.11 \mu\text{m}$. As mentioned previously, the spectral bands centered at these two wavelengths can be used for inferring cloud effective particle size (D_e) and optical thickness (τ). The results in Fig. 16 indicate that the phase function values at scattering angles near 180° are much lower for hollow bullet rosettes than for solid bullet rosettes. For small effective particle sizes (e.g., $D_e = 35 \mu\text{m}$), the 22° halo peak is not pronounced for hollow bullet rosettes, but the halo becomes better defined as particle size increases (e.g., $D_e = 135 \mu\text{m}$). These results suggest that the phase function associated with a population of hollow bullet rosettes is more sensitive to the effective particle size than its solid counterpart at visible and near-infrared wavelengths.

To investigate the effects of hollow bullet rosettes on the retrieval of D_e and τ , two sets of lookup tables (LUT) based on the bulk scattering properties of hollow and solid bullet rosettes are computed from the Discrete Ordinates Radiative Transfer (DISORT) model developed by Stamnes et al. (1988). A Lambertian surface with an albedo of 0.03 is assumed for calculations over ocean. Bullet rosettes are assumed to have 11 branches with aspect ratios as specified by Eq.

(3). Figure 17 shows the comparison of the two sets of LUTs for two sun-satellite configurations. The dashed maroon lines in Fig. 17 indicate the LUT for solid ($\beta = 0.0$) bullet rosettes and the solid blue lines indicate the LUT for hollow ($\beta = 1.0$) bullet rosettes. The top panel of Fig. 17 shows a case with a solar zenith angle of $\theta_0 = 30^\circ$ and a viewing zenith angle of $\theta = 0^\circ$ (note that the view azimuth angle is not required for specifying the observed radiance in this case). For the bottom panel of Fig. 17, the solar zenith angle, the satellite-viewing zenith angle, and the relative azimuth angle between the sun and satellite are 26° , 40° , and 42° , respectively.

It is evident from the LUTs shown in Fig. 17 that retrievals based on hollow bullet rosettes will result in larger values of optical thickness and smaller values of effective particle size in comparison with the retrievals based on solid bullet rosettes. To illustrate this, consider a pair of radiances for the two bands centered at 0.86 and $2.11 \mu\text{m}$, which are denoted by the red dots in Fig. 17. For the red dot in the top panel, the inferred optical thickness and effective size is 7.8 and $34 \mu\text{m}$, respectively, if hollow bullet rosettes are assumed. However, the inferred optical thickness and effective size is 5.2 and $60 \mu\text{m}$, respectively, if solid bullet ro-

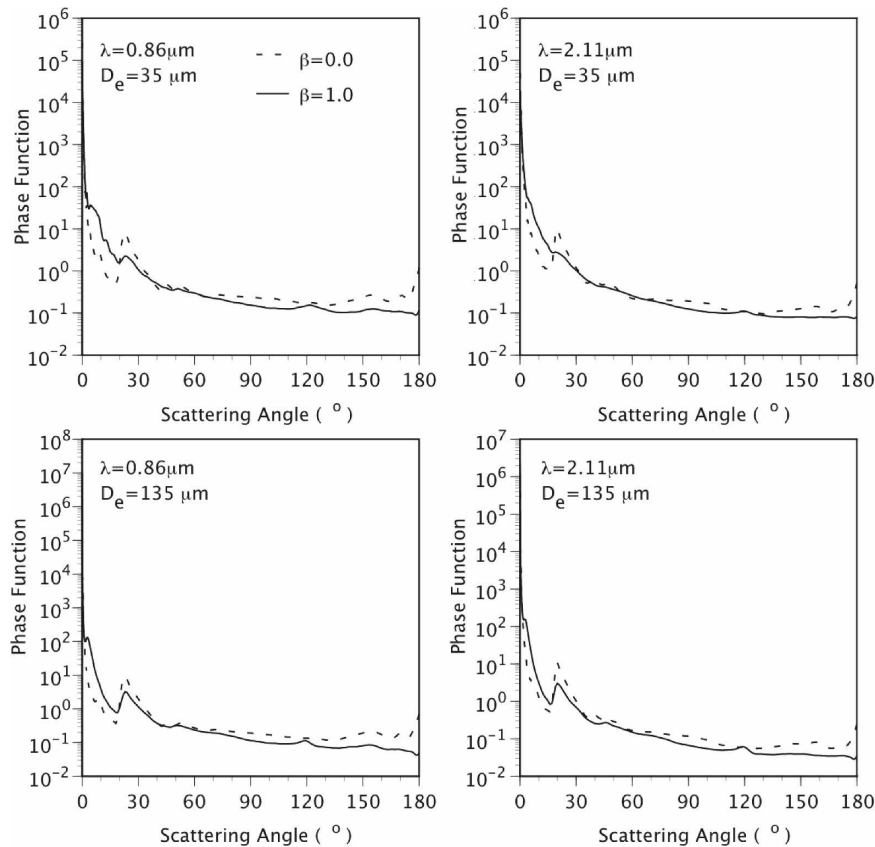


FIG. 16. Scattering phase function of hollow bullet rosettes at wavelengths of (left) 0.86 and (right) 2.11 μm for effective particle size (top) $D_e = 35 \mu\text{m}$ and (bottom) $D_e = 135 \mu\text{m}$.

settes are assumed. For the red dot in the bottom panel, the retrieval values based on hollow and solid bullet rosettes are ($\tau = 7.8$, $D_e = 34 \mu\text{m}$) and ($\tau = 6.2$, $D_e = 52 \mu\text{m}$), respectively. From the example shown in Fig. 17, it is obvious that the optical effects resulting from the hollow structures in bullet rosettes can have an important implication for the remote sensing of ice cloud properties from measurements at visible and near-infrared wavelengths.

5. Summary

We compute the complete phase matrix of randomly oriented hollow bullet rosette ice particles using the improved geometric optics method previously developed by Yang and Liou (1996b). A hollow bullet rosette ice particle is assumed to have between 2 and 12 branches with a hollow structure at the end of each bullet; each hollow structure extends into the bullet and has a pyramidal tip. We also discuss the bulk optical properties of a population of hollow bullet rosette ice particles in comparison with their solid counterparts.

In comparison with solid bullet rosettes, the primary optical effect of including hollow structures in each bullet is to decrease the amount of backscattering in the phase function. The magnitude of the decrease of backscattering is sensitive to the depths of hollow ends. Conversely, the magnitude of the forward scattering in the phase function is higher for hollow bullet rosettes than for their solid counterparts. The asymmetry factor is larger for hollow bullet rosettes than for solid bullet rosettes. Simulations are performed at two wavelengths, 0.86 and 2.11 μm , to investigate the differences between hollow and solid bullet rosettes and investigate the impact of the habit on the inference of effective particle size and optical thickness. With a bispectral technique based on these two wavelengths, we find that use of hollow bullet rosettes results in larger value of optical thickness and a smaller effective particle size in comparison with the case of solid bullet rosettes.

For active lidar measurements, the depolarization ratio is of great importance. The depolarization ratio for hollow bullet rosettes is much lower than its counterpart in the solid case. Moreover, the behavior of the

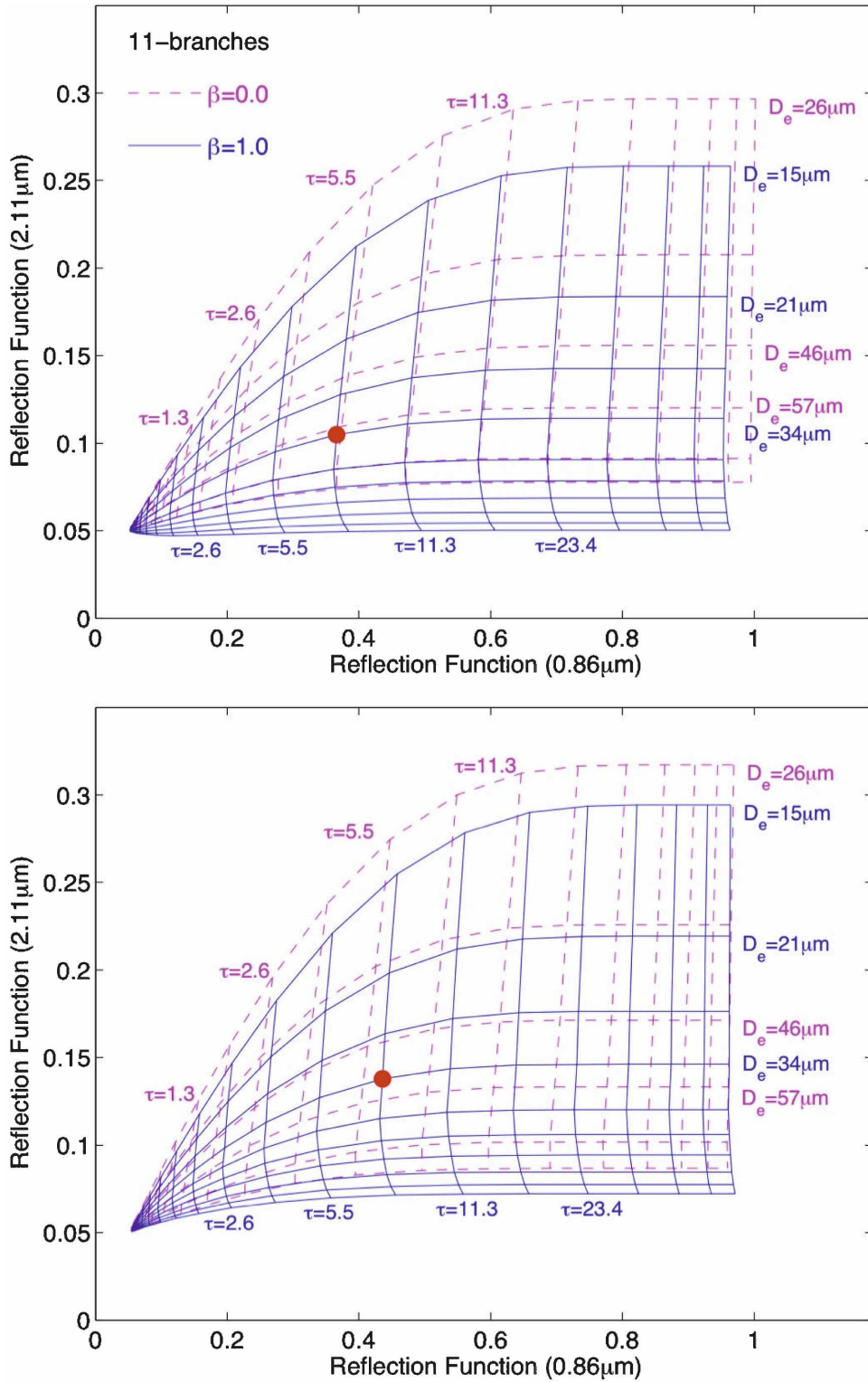


FIG. 17. Correlation between 2.11- and 0.86- μm reflectance over ocean for two sun-satellite configurations. The red dots indicated pairs of the reflectances at 0.86 and 2.11 μm , which are assumed to be “measurements” used for retrieving cloud optical thickness and effective particle size. The solar and view zenith angles are (top) 30° and 0°, respectively, and (bottom) 26° and 40°, respectively. The relative azimuth angle is 42°. A value of 0.03 is assumed for sea surface albedo.

depolarization ratio as a function of the effective particle size is significantly different for solid and hollow bullet rosettes.

In future work, we will extend this study to further examine the implications of the hollow bullet rosette habit to ice cloud properties inferred from infrared hyperspectral measurements as well as from other sensors.

Acknowledgments. Ping Yang's research is supported by the National Science Foundation Physical Meteorology Program (ATM-0239605), and a research grant (NNL06AA23G) from the National Aeronautics and Space Administration (NASA). George Kattawar's research is supported by the Office of Naval Research under Contracts N00014-02-1-0478 and N00014-06-1-0069.

REFERENCES

- Arnott, W. P., Y. Dong, J. Hallett, and M. R. Poellot, 1994: Role of small ice crystals in radiative properties of cirrus: A case study, FIRE II, November 22, 1991. *J. Geophys. Res.*, **99**, 1371–1381.
- Baran, A. J., P. Yang, and S. Havemann, 2001: Calculation of the single-scattering properties of randomly oriented hexagonal ice columns: A comparison of the T-matrix and the finite-difference time-domain methods. *Appl. Opt.*, **40**, 4376–4386.
- Baum, B. A., A. J. Heymsfield, P. Yang, and S. M. Bedka, 2005a: Bulk scattering properties for the remote sensing of ice clouds. I: Microphysical data and models. *J. Appl. Meteor.*, **44**, 1885–1895.
- , P. Yang, A. J. Heymsfield, S. Platnick, M. D. King, Y. X. Hu, and S. M. Bedka, 2005b: Bulk scattering properties for the remote sensing of ice clouds. II: Narrowband models. *J. Appl. Meteor.*, **44**, 1896–1911.
- Besson, L., 1923: Concerning haloes of abnormal radii. *Mon. Wea. Rev.*, **51**, 254–255.
- Cai, Q., and K. N. Liou, 1982: Polarized light scattering by hexagonal ice crystals: Theory. *Appl. Opt.*, **21**, 3569–3580.
- Chang, P. C., J. G. Walker, and K. I. Hopcraft, 2005: Ray tracing in absorbing media. *J. Quant. Spectrosc. Radiat. Transfer*, **96**, 327–341.
- C.-Labonnote, L., G. Brogniez, M. Doutriaux-Boucher, J.-C. Buriez, J.-F. Gayet, and H. Chepfer, 2000: Modeling of light scattering in cirrus clouds with inhomogeneous hexagonal monocrystals: Comparison with in-situ and ADEOS-POLDER measurements. *Geophys. Res. Lett.*, **27**, 113–116.
- , —, J.-C. Buriez, M. Doutriaux-Boucher, J.-F. Gayet, and A. Macke, 2001: Polarized light scattering by inhomogeneous hexagonal monocrystals: Validation with ADEOS-POLDER measurements. *J. Geophys. Res.*, **106**, 12 139–12 153.
- Draine, B. T., and P. J. Flatau, 1994: Discrete-dipole approximation for scattering calculations. *J. Opt. Soc. Amer. A*, **11**, 1491–1499.
- Foot, J. S., 1988: Some observations of the optical properties of clouds. II: Cirrus. *Quart. J. Roy. Meteor. Soc.*, **114**, 145–164.
- Fu, Q., 2007: Generalized parameterization of asymmetry factor of cirrus clouds for climate models. *J. Atmos. Sci.*, **64**, 4140–4150.
- , P. Yang, and W. B. Sun, 1998: An accurate parameterization of the infrared radiative properties of cirrus clouds for climate models. *J. Climate*, **11**, 2223–2237.
- Goldie, E. C. W., G. T. Meaden, and R. White, 1976: The concentric halo display of 14 April 1974. *Weather*, **31**, 304–311.
- Greenler, R., 1980: *Rainbows, Halos, and Glories*. Cambridge University Press, 195 pp.
- Grenfell, T. C., S. P. Neshyba, and S. G. Warren, 2005: Representation of a nonspherical ice particle by a collection of independent spheres for scattering and absorption of radiation: 3. Hollow columns and plates. *J. Geophys. Res.*, **110**, D17203, doi:10.1029/2005JD005811.
- Hess, M., and M. Wiegner, 1994: COP: A data library of optical properties of hexagonal ice crystals. *Appl. Opt.*, **33**, 7740–7746.
- Hu, Y., and Coauthors, 2007: The depolarization-attenuated backscatter relation: CALIPSO lidar measurements vs. theory. *Opt. Express*, **15**, 5327–5332.
- Heymsfield, A. J., S. Lewis, A. Bansemer, J. Iaquinta, L. M. Miloshevich, M. Kajikawa, C. Twohy, and M. R. Poellot, 2002: A general approach for deriving the properties of cirrus and stratiform ice cloud particles. *J. Atmos. Sci.*, **59**, 3–29.
- Iaquinta, J., H. Isaka, and P. Personne, 1995: Scattering phase function of bullet rosette ice crystals. *J. Atmos. Sci.*, **52**, 1401–1413.
- Jacobowitz, H., 1971: A method for computing the transfer of solar radiation through clouds of hexagonal ice crystals. *J. Quant. Spectrosc. Radiat. Transfer*, **11**, 691–695.
- Kahnert, F. M., 2003: Numerical methods in electromagnetic scattering theory. *J. Quant. Spectrosc. Radiat. Transfer*, **79–80**, 775–824.
- Key, J. R., P. Yang, B. A. Baum, and S. L. Nasiri, 2002: Parameterization of shortwave ice cloud optical properties for various particle habits. *J. Geophys. Res.*, **107**, 4181, doi:10.1029/2001JD000742.
- King, M. D., S. Platnick, P. Yang, G. T. Arnold, M. A. Gray, J. C. Riedi, S. A. Ackerman, and K. N. Liou, 2004: Remote sensing of liquid water and ice cloud optical thickness, and effective radius in the Arctic: Application of airborne multispectral MAS data. *J. Atmos. Oceanic Technol.*, **21**, 857–875.
- Kobayashi, T., Y. Furukawa, K. T. Takahashi, and H. Uyeda, 1976: Cubic structure models at the junctions in polycrystalline snow crystals. *J. Cryst. Growth*, **35**, 262–267.
- Liou, K. N., 1986: Influence of cirrus clouds on weather and climate process: A global perspective. *Mon. Wea. Rev.*, **114**, 1167–1199.
- Lynch, D. K., K. Sassen, D. O'C. Starr, and G. Stephens, Eds., 2002: *Cirrus*. Oxford University Press, 480 pp.
- Macke, A., 1993: Scattering of light by polyhedral ice crystals. *Appl. Opt.*, **32**, 2780–2788.
- , M. I. Mishchenko, K. Muinonen, and B. E. Carlson, 1995: Scattering of light by large nonspherical particles: Ray-tracing approximation versus T-matrix method. *Opt. Lett.*, **20**, 1934–1936.
- , —, and B. Cairns, 1996a: The influence of inclusions on light scattering by large ice particles. *J. Geophys. Res.*, **101**, 23 311–23 316.
- , J. Mueller, and E. Raschke, 1996b: Single scattering properties of atmospheric ice crystal. *J. Atmos. Sci.*, **53**, 2813–2825.

- McFarquhar, G. M., P. Yang, A. Macke, and A. J. Baran, 2002: A new parameterization of single-scattering solar radiative properties for tropical anvils using observed ice crystal size and shape distributions. *J. Atmos. Sci.*, **59**, 2458–2478.
- Minnis, P., P. W. Heck, and D. F. Young, 1993a: Inference of cirrus cloud properties using satellite-observed visible and infrared radiances. Part II: Verification of theoretical cirrus radiative properties. *J. Atmos. Sci.*, **50**, 1305–1322.
- , Y. Takano, and K.-N. Liou, 1993b: Inference of cirrus cloud properties using satellite-observed visible and infrared radiances. Part I: Parameterization of radiance fields. *J. Atmos. Sci.*, **50**, 1279–1304.
- Mishchenko, M. I., and L. D. Travis, 1994: Light scattering by polydispersions of randomly oriented spheroids with sizes comparable to wavelengths of observations. *Appl. Opt.*, **33**, 7206–7225.
- , and A. Macke, 1998: Incorporation of physical optics effects and computations of the Legendre expansion for ray-tracing phase functions involving delta-function transmission. *J. Geophys. Res.*, **103**, 1799–1805.
- , and K. Sassen, 1998: Depolarization of lidar returns by small ice crystals: An application to contrails. *Geophys. Res. Lett.*, **25**, 309–312, doi:10.1029/97GL03764.
- , and A. Macke, 1999: How big should hexagonal ice crystals be to produce halos? *Appl. Opt.*, **38**, 1626–1629.
- , W. J. Wiscombe, J. W. Hovenier, and L. D. Travis, 2000: Overview of scattering by nonspherical particles. *Light Scattering by Nonspherical Particles: Theory, Measurements, and Geophysical Applications*, M. I. Mishchenko, J. W. Hovenier, and L. D. Travis, Eds., Academic Press, 29–60.
- Mitchell, D. L., and W. P. Arnott, 1994: A model predicting the evolution of ice particle size spectra and radiative properties of cirrus clouds. Part II: Dependence of absorption and extinction on ice crystal morphology. *J. Atmos. Sci.*, **51**, 817–832.
- , A. J. Baran, W. P. Arnott, and C. Schmitt, 2006: Testing and comparing the modified anomalous diffraction approximation. *J. Atmos. Sci.*, **63**, 2948–2962.
- Muunonen, K., 1989: Scattering of light by crystals: A modified Kirchhoff approximation. *Appl. Opt.*, **28**, 3044–3050.
- Nakajima, T., and M. D. King, 1990: Determination of the optical thickness and effective particle radius of clouds from reflected solar radiation measurements. Part I: Theory. *J. Atmos. Sci.*, **47**, 1878–1893.
- Platnick, S., M. D. King, S. A. Ackerman, W. P. Menzel, B. A. Baum, J. C. Riédi, and R. A. Frey, 2003: The MODIS cloud products: Algorithms and examples from Terra. *IEEE Trans. Geosci. Remote Sens.*, **41**, 459–473.
- Rockwitz, K.-D., 1989: Scattering properties of horizontally oriented ice crystal columns in cirrus clouds. *Appl. Opt.*, **28**, 4103–4110.
- Schmitt, C. G., and A. J. Heymsfield, 2007: On the occurrence of hollow bullet rosette and column shaped ice crystals in mid-latitude cirrus. *J. Atmos. Sci.*, **64**, 4515–4520.
- , J. Iaquinta, and A. J. Heymsfield, 2006: The asymmetry parameter of cirrus clouds composed of hollow bullet rosette-shaped ice crystals from ray-tracing calculations. *J. Appl. Meteor. Climatol.*, **45**, 973–981.
- Stamnes, K., S.-C. Tsay, W. Wiscombe, and K. Jayaweera, 1988: Numerically stable algorithm for discrete-ordinate-method radiative transfer in multiple scattering and emitting layered media. *Appl. Opt.*, **27**, 2502–2509.
- Stephens, G. L., S. C. Tsay, P. W. Stackhouse, and P. J. Flatau, 1990: The relevance of the microphysical and radiative properties of cirrus clouds to climate and climate feedback. *J. Atmos. Sci.*, **47**, 1742–1753.
- Sun, W., Q. Fu, and Z. Chen, 1999: Finite-difference time-domain solution of light scattering by dielectric particles with perfectly matched layer absorbing boundary conditions. *Appl. Opt.*, **38**, 3141–3151.
- Takano, Y., and K. Jayaweera, 1985: Scattering phase matrix for hexagonal ice crystals computed from ray optics. *Appl. Opt.*, **24**, 3254–3263.
- , and K. N. Liou, 1989: Solar radiative transfer in cirrus clouds. Part I: Single-scattering and optical properties of hexagonal ice crystals. *J. Atmos. Sci.*, **46**, 3–19.
- , and —, 1995: Radiative transfer in cirrus clouds. Part III: Light scattering by irregular ice crystals. *J. Atmos. Sci.*, **52**, 818–837.
- Taflove, A., 1995: *Computational Electrodynamics: The Finite-Difference Time-Domain Method*. Artech House, 599 pp.
- Tape, W., 1994: *Atmospheric Halos*. Antarctic Research Series, Vol. 64, Amer. Geophys. Union, 143 pp.
- , and J. Moilanen, 2006: *Atmospheric Halos and the Search for Angle X*. American Geophysical Union, 238 pp.
- Um, J., and G. M. McFarquhar, 2007: Single-scattering properties of aggregates of bullet rosettes in cirrus. *J. Appl. Meteor. Climatol.*, **46**, 757–775.
- Walden, V. P., S. G. Warren, and E. Tuttle, 2003: Atmospheric ice crystals over the Antarctic Plateau in winter. *J. Appl. Meteor.*, **42**, 1391–1405.
- Wendisch, M., P. Yang, and P. Pilewskie, 2007: Effects of ice crystal habit on the thermal infrared radiative properties and forcing of cirrus clouds. *J. Geophys. Res.*, **112**, D08201, doi:10.1029/2006JD007899.
- Wendling, P., R. Wendling, and H. K. Weickmann, 1979: Scattering of solar radiation by hexagonal ice crystals. *Appl. Opt.*, **18**, 2663–2671.
- Wielgaard, D. J., M. I. Mishchenko, A. Macke, and B. E. Carlson, 1997: Improved T-matrix computations for large, nonabsorbing and weakly absorbing nonspherical particles and comparison with geometrical-optics approximation. *Appl. Opt.*, **36**, 4305–4313.
- Winker, D. M., W. H. Hunt, and M. J. McGill, 2007: Initial performance assessment of CALIOP. *Geophys. Res. Lett.*, **34**, L19803, doi:10.1029/2007GL030135.
- Yang, P., and K. N. Liou, 1996a: Finite-difference time domain method for light scattering by small ice crystals in three-dimensional space. *J. Opt. Soc. Amer. A.*, **13**, 2072–2085.
- , and —, 1996b: Geometric-optics-integral-equation method for light scattering by nonspherical ice crystals. *Appl. Opt.*, **35**, 6568–6584.
- , and —, 1998: Single-scattering properties of complex ice crystals in terrestrial atmosphere. *Contrib. Atmos. Phys.*, **71**, 223–248.
- , and —, 2006: Light scattering and absorption by nonspherical ice crystals. *Light Scattering Reviews: Single and Multiple Light Scattering*, A. Kokhanovsky, Ed., Springer-Praxis, 31–71.
- , B.-C. Gao, B. A. Baum, W. Wiscombe, M. I. Mishchenko, D. M. Winker, and S. L. Nasiri, 2001: Asymptotic solutions of optical properties of large particles with strong absorption. *Appl. Opt.*, **40**, 1532–1547.
- , H. L. Wei, G. W. Kattawar, Y. X. Hu, D. M. Winker, C. A. Hostetler, and B. A. Baum, 2003: Sensitivity of the backscat-

- tering Mueller matrix to particle shape and thermodynamic phase. *Appl. Opt.*, **42**, 4389–4395.
- , and Coauthors, 2007: Modeling of the scattering and radiative properties of nonspherical dust particles. *J. Aerosol Sci.*, **38**, 995–1014.
- Yee, S. K., 1966: Numerical solution of initial boundary value problems involving Maxwell's equations in isotropic media. *IEEE Trans. Antennas Propag.*, **14**, 302–307.
- Zhang, M. H., and Coauthors, 2005: Comparing clouds and their seasonal variations in 10 atmospheric general circulation models with satellite measurements. *J. Geophys. Res.*, **110**, D15S02, doi:10.1029/2004JD005021.
- Zhang, Z., P. Yang, G. W. Kattawar, S.-C. Tsay, B. A. Baum, Y. Hu, A. J. Heymsfield, and J. Reichardt, 2004: Geometrical-optics solution to light scattering by droxtal ice crystals. *Appl. Opt.*, **43**, 2490–2499.